

A Nanoparticle-Based Model Delivery System To Guide the Rational Design of Gene Delivery to the Liver. 1. Synthesis and Characterization

Stephen R. Popielarski, Suzie H. Pun,[†] and Mark E. Davis*

Chemical Engineering, California Institute of Technology, Pasadena, California 91125. Received April 14, 2005

Nonviral gene delivery systems are amenable to forming colloidal particles with a wide range of physicochemical properties that include size, surface charge, and density and type of ligand presented. However, it is not known how to best design these particles without having a set of physicochemical design constraints that have been optimized for the intended gene delivery application. Here, a nanoparticle-based model delivery system is developed that can mimic the surface properties of nonviral gene delivery particles, and this model system is used to define design constraints that should be applied to next generation gene delivery particles. As a test case, a well-defined nanoparticle-based system is developed to guide the rational design of gene delivery to hepatocytes in the liver. The synthetic scheme utilizes monodisperse polystyrene particles and provides for variation of mean particle size and particle size distribution through variation in reaction conditions. The nanoparticles are PEGylated to provide stability in serum and also incorporate targeting ligands, e.g., galactose, at tunable densities. Four nanoparticles are synthesized from uniformly sized polystyrene beads specifically for the purpose of identifying design constraints to guide next generation gene delivery to the liver. These four nanoparticles are Gal-50 and Gal-140, that are galactosylated 50 and 140 nm nanoparticles, and MeO-50 and MeO-140, that are methoxy-terminated 50 and 140 nm nanoparticles. All four particles have the same surface charge, and Gal-50 and Gal-140 have the same surface galactose density. The availability of galactose ligands to receptor binding is demonstrated here by agglutination with RCA₁₂₀.

INTRODUCTION

Gene therapy promises to revolutionize the clinical treatment of countless genetic disorders (1), including many diseases of the liver (2). Though human gene therapy of liver diseases is still in its infancy, preclinical studies in animal models of disease have demonstrated proof of concept results in nearly all varieties of liver diseases that are conceptually amenable to gene therapy treatment (3–6).

However, numerous investigators have identified the importance of carefully designing and controlling the properties of gene delivery systems for selectively targeting the liver. A prerequisite to selective targeting is particle stability in vivo and the minimization of non-specific uptake. We and others have previously demonstrated the importance of PEGylation (PEG: poly(ethylene glycol)) to stabilize polyplexes and to reduce their nonspecific uptake (7). Nonspecific uptake of particles is commonly due to rapid clearance by cells of the mononuclear phagocytic system (8) and adhesion to the endothelial lining of the vascular system (9). Such undesirable uptake is minimized by surfaces with little or no protein adsorption. In particular, certain proteins called opsonins interact with phagocyte receptors and promote recognition by scavenger cells of the reticuloendothelial organs. Phagocytosis is frequently initiated by adsorption of opsonins onto the surface of particles followed by complement activation or other recognition,

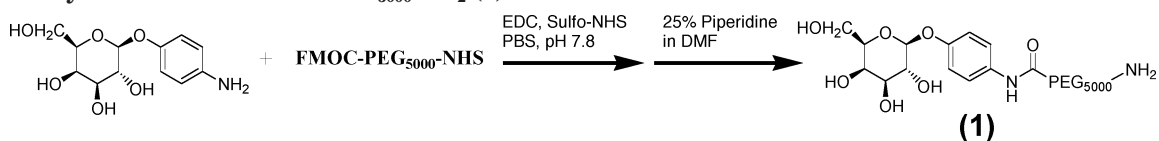
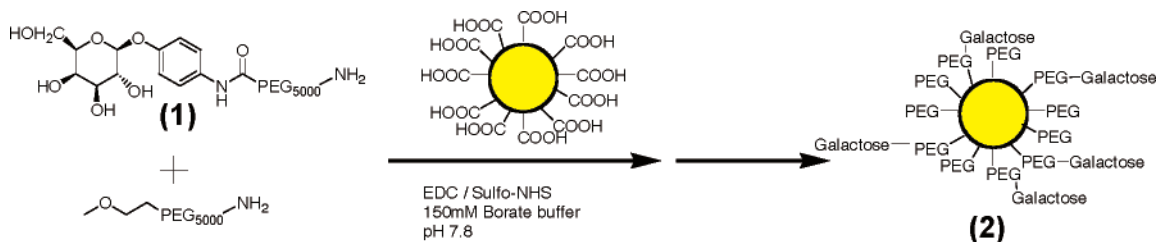
leading to internalization by macrophages and intracellular processing. Dunn et al. (10) have demonstrated that interaction of PEGylated polystyrene nanoparticles with nonparenchymal liver cells in vitro decreased with higher surface densities of PEG and also resulted in longer circulation times following intravenous injection into rats.

By formulating PEGylated cyclodextrin-based gene-delivery particles under different conditions, the size, surface charge, and ligand density of the final gene delivery particle can all readily be adjusted (11). However, the power of this flexibility cannot be maximized without a set of physicochemical design constraints that have been optimized for the intended gene-delivery application. In particular, we are interested in generating a set of design requirements to guide gene delivery to the liver. In this pursuit, we describe herein the development of a nanoparticle-based model system that will facilitate the systematic identification of relevant physicochemical properties that alter the hepatic distribution of nanoparticles. Further, this nanoparticle-based model is intended to mimic the surface properties achievable with nonviral delivery systems but specifically with the linear, cyclodextrin-based gene delivery system developed in our laboratory (12–15). As such, the model system will be PEGylated and must facilitate variation of parameters such as particle size, surface charge, and ligand type and density.

In the present work, we detail the synthesis and characterization of PEGylated nanoparticles with tunable physicochemical properties. The synthesized nanoparticles are slightly anionic to minimize nonspecific uptake in vivo, and galactose will be used as a targeting ligand since galactose receptors in vivo are almost exclusively

* To whom correspondence should be addressed. E-mail: mdavis@cheme.caltech.edu.

[†] Current address: Department of Bioengineering, University of Washington, Box 352255, Seattle, WA 98195.

Scheme 1. Synthesis of Galactose-PEG₅₀₀₀-NH₂ (1)**Scheme 2. Synthesis of PEGylated Nanoparticles (2)**

found in the liver. In particular, four nanoparticles will be described that are appropriate for uptake experiments: Gal-50 and Gal-140 are galactosylated nanoparticles with diameters of 50 and 140 nm, while MeO-50 and MeO-140 are methoxy-terminated 50 and 140 nm nanoparticles. Through the use of these nanoparticles, the effects of nanoparticle size and surface presentation of galactose on hepatic distribution in mice can be explored, and the results of *in vitro* and *in vivo* uptake experiments are presented in Part 2 of our work (16).

MATERIALS AND METHODS

Fmoc-PEG₅₀₀₀-NHS was purchased from Nektar (San Carlos, CA) and used as received. All other reagents and solvents were obtained from commercial suppliers and were used as received, unless specifically noted. Matrix-assisted, laser desorption/ionization time-of-flight mass spectroscopy (MALDI-TOF) was performed on a PerSeptive Biosystems Voyager DE PRO BioSpectrometry Workstation (PerSeptive Biosystems; Framingham, MA) in the positive ion mode using a 2,5-dihydroxy benzoic acid matrix. HPLC was performed on an Agilent 1100 Series HPLC (Agilent Technologies; Palo Alto, CA) with a Prevail C18 5 μ m column (Alltech; Deerfield, IL) and a SEDEX Model 75 Evaporative Light Scattering (ELS) detector (Richard Scientific; Novato, CA).

Synthesis of Galactose-PEG₅₀₀₀-amine. (1, Scheme 1). 4-Aminophenyl β -D-galactopyranoside (1.79 g, 6.38 mmol) and Fmoc-PEG₅₀₀₀-NHS (2.17 g, 0.43 mmol) were dissolved in about 16 mL of phosphate-buffered saline (PBS, pH 7.4, 137 mM sodium chloride, 10 mM phosphate, 2.7 mM potassium chloride). Sulfo-NHS (97 mg, 0.44 mmol) was added, the pH was adjusted to pH 7.8, and the reaction was stirred at ambient temperature. After 6 h, EDC was added (435 mg, 2.27 mmol), and the reaction was stirred for an additional 48 h. The crude reaction mixture was dialyzed in 500 molecular-weight cutoff (MWCO) Float-A-Lyzers (Pierce; Rockford, IL) against water for 2 days with twice daily dialysate changes. The solution was dried on a rotary evaporator at temperatures not exceeding 35 °C. Deprotection of the amine was accomplished by stirring the off-white product in 50 mL of 25% piperidine in DMF for 4 h at room temperature. The solution was then concentrated under reduced pressure at temperatures not exceeding 40 °C. The viscous liquid was transferred to polypropylene centrifuge tubes and water was added. Centrifugation and filtration through a 0.2 μ m HT Tuffryn Membrane filter (VWR; West Chester, PA) resulted in complete Fmoc removal from the crude reaction mixture. The solution was subjected to extensive dialysis in 500

MWCO Float-A-Lyzers before being lyophilized to dryness. Purity was confirmed by HPLC-ELS and MALDI-TOF mass spectroscopy. Final yield: 1.25 g, 59%.

Synthesis of PEGylated-polystyrene Nanoparticles. (2, Scheme 2). Fluorescein-embedded PEGylated-polystyrene nanoparticles were synthesized by reaction of Fluospheres (Molecular Probes; Eugene, OR) with MeO-PEG₅₀₀₀-NH₂ or Galactose-PEG₅₀₀₀-NH₂ (1). Two sizes of Fluospheres were used as starting materials in this work. Fluospheres (28 nm) were used to synthesize PEGylated nanoparticles with final diameters up to 60 nm, while nanoparticles up to 160 nm were synthesized by PEGylation of 105 nm Fluospheres. Fluospheres (28 nm) were sonicated then centrifuged at 14 000g for 20 min prior to use. All Fluospheres were sonicated immediately before being added to reaction vials. Typically, 500 μ L of a 2% Fluosphere suspension (3.21 μ mol COOH for 105 nm Fluospheres) is added to 32 mg of MeO-PEG₅₀₀₀-NH₂ (6.42 μ mol) in a 1.5 mL Eppendorf tube and mixed to dissolve the PEG. Sulfo-NHS (6.3 mg) (Pierce) is added to each tube, and 200 mM borate buffer, pH 8.2, is added up to 1 mL total volume per tube. The pH of each reaction tube is adjusted to pH 7.80, and then 1.0 mg of EDC (5.13 mmol) is added to each tube and vortex mixed for 6 h. Purification of 50 nm nanoparticles was accomplished by dialysis in 100k MWCO DispoDialyzers (Pierce) against a variety of salt solutions starting with 3 M NaCl and ending with PBS. A minimum of seven dialysate changes were performed until no free PEG was detected by HPLC-ELS. Workup of 140 nm nanoparticles was accomplished by cold centrifugation and repeated washes in salt solutions ranging from 4 M NaCl to final resuspension in PBS. Bead concentrations were determined by comparison to fluorescence of known concentrations of as-received Fluospheres on a SpectraFluor Plus fluorescence plate reader (Tecan; Research Triangle Park, NC) with FITC filters (ex: 485 nm; em: 530 nm). Yields: 50 nm nanoparticles, typically 40%; 140 nm nanoparticles, typically 70%.

Particle Size and ζ -Potential Measurements. Colloidal particle size was determined by photon correlation spectroscopy in 150 mM NaCl at a wavelength of 532 nm, scattering angle of 90°, and refractive index of 1.59 using a ZetaPALS instrument (Brookhaven Instruments; Holtsville, NY). Ten measurements on each diluted nanoparticle sample were taken, and the mean hydrodynamic diameter was reported. Nanoparticles (50 nm) were typically measured at 1×10^{13} particles/mL while 140 nm nanoparticles were typically measured at 1.5×10^{10} particles/mL. ζ -Potential measurements were calculated from electrophoretic mobilities using the Smoluchowski

equation. Nanoparticle electrophoretic mobilities were measured in 150 mM NaCl using a ZetaPALS instrument with the following conditions: fluid refractive index 1.334, electric field 5.41 V/cm and adjusted to a conductance of 15.0 mS. Three samples were each measured seven times, and the mean \pm standard deviation of each was reported.

Determination of Galactose Surface Density. Concentration of galactose on the surface of nanoparticles was determined with the Amplex Red Galactose/Galactose Oxidase Assay Kit (Molecular Probes; Eugene, OR) by comparison to standard curves of galactose in solution with unmodified polystyrene beads. The reaction was allowed to proceed for a minimum of 120 min before final absorbance readings were taken due to the different rates of reaction of galactose oxidase with galactose in solution versus with surface-immobilized galactose.

RCA₁₂₀ Lectin Agglutination. A suspension of 5.4×10^{12} nanoparticles in 500 μ L of PBS was added to 4.7×10^{14} molecules of RCA₁₂₀ lectin (Sigma-Aldrich; St. Louis, MO) in 500 μ L of PBS. Each lectin has two identical binding sites, for a total of 9.5×10^{14} galactose binding sites per experiment. Agglutination was monitored by measurement of absorbance at 560 nm. After 30 min, 8×10^{18} molecules of galactose were added in 100 μ L of PBS to disaggregate the system.

TEM of Nanoparticles. Nanoparticles in water were applied to 400-mesh, freshly glow-discharged, carbon-coated copper grids for 45 s. After this time, excess water was removed by blotting with filter paper, and the sample was negatively stained with 2% uranyl acetate for 45 s before blotting. A Philips 201 electron microscope, operated at 80 kV, was used to record images.

Serum-Induced Nanoparticle Aggregation. Mouse serum (Sigma) was incubated in 96-well plates at 37 °C and 5% CO₂ for a minimum of 2 h before use. Nanoparticles (5×10^{10}) were added to each 90 μ L of equilibrated sera, and aggregation was monitored by measurement of absorbance at 560 nm at 37 °C.

RESULTS AND DISCUSSION

Gal-PEG₅₀₀₀-NH₂ Synthesis and Characterization. Fmoc-PEG₅₀₀₀-NHS was converted to high-purity Gal-PEG₅₀₀₀-NH₂. The reaction was driven to completion by a large excess of 4-aminophenyl β -D-galactopyranoside and an additional dosing of carbodiimide coupling agent, EDC. Optimum reaction pH in NHS-mediated peptide coupling reactions is a tradeoff between the amide formation rate and the rate of hydrolysis of the activated NHS-ester. PEG₅₀₀₀-NH₂ has a pK_a of about 9.2 (17) and NHS-esters on the PEG chains deactivate quickly, especially above a pH of about 8. An optimal pH of about 7.8 was determined for this reaction. While the concentration of Fmoc-PEG₅₀₀₀-NHS did not significantly influence reaction yield, supplementation with additional Sulfo-NHS and EDC was necessary to reactivate any carboxylic esters on the PEG that had hydrolyzed.

The purity of the final purified compound was determined by HPLC-ELS, as shown in Figure 1. Peaks representing starting materials (Figure 1a) and intermediates were resolved relative to the Gal-PEG₅₀₀₀-NH₂ peak (Figure 1b). Purity was typically greater than 98%, as determined by HPLC.

MALDI-TOF mass spectroscopy also confirmed that the reaction went to completion. Primary peaks in the MALDI-TOF spectra (Figure 2) line up well with predicted molecular weights (Table 1) of Fmoc-PEG₅₀₀₀-NHS

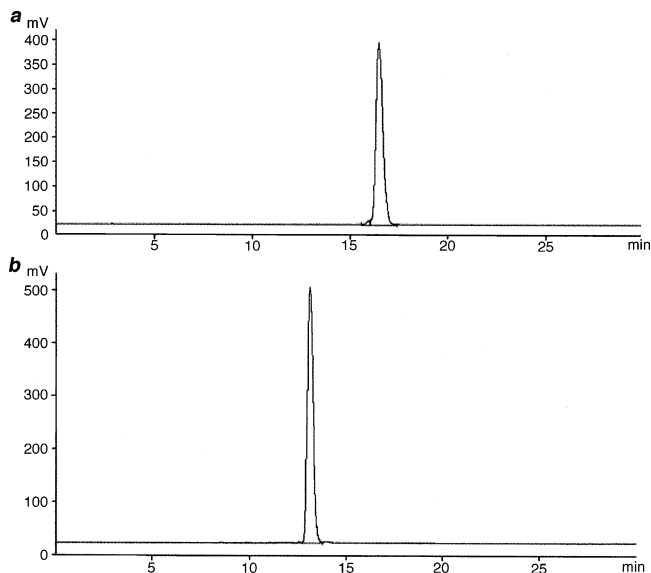


Figure 1. HPLC spectra of (a) Fmoc-PEG₅₀₀₀-COOH and (b) Gal-PEG₅₀₀₀-NH₂.

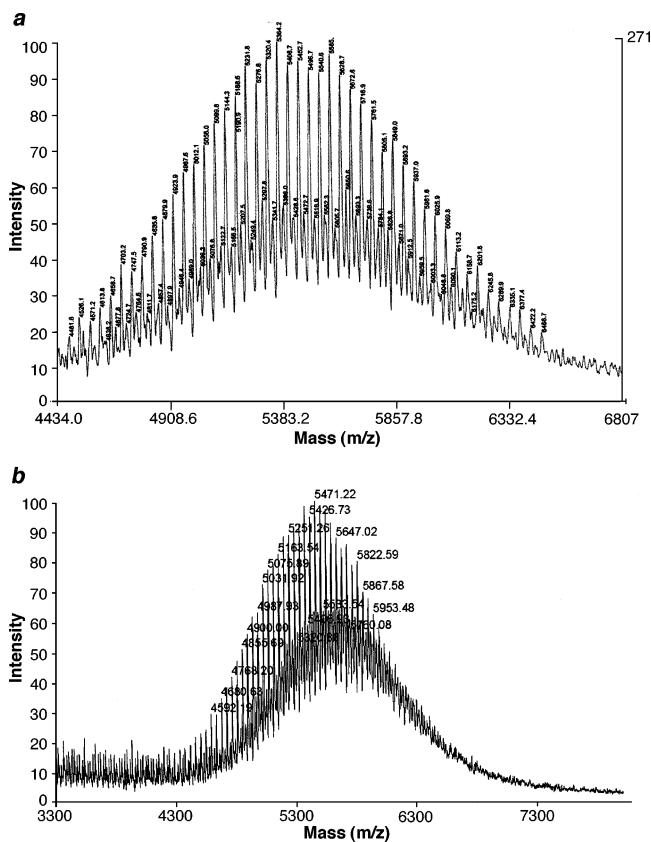


Figure 2. MALDI-TOF mass spectra of (a) Fmoc-PEG₅₀₀₀-NHS and (b) Gal-PEG₅₀₀₀-NH₂.

(Figure 2a) and Gal-PEG₅₀₀₀-NH₂ (Figure 2b), according to the following formulas:

$$MW_{\text{Fmoc-PEG-NHS}} = 44.026n + \frac{170.042}{[\text{EO repeat}]} + \frac{238.082}{[\text{NH-Fmoc}]}$$

$$MW_{\text{Gal-PEG-NH}_2} = 44.026n + \frac{326.354}{[(\text{CH}_2)_2\text{C(O)-Gal}]} + \frac{16.023}{[\text{NH}_2]}$$

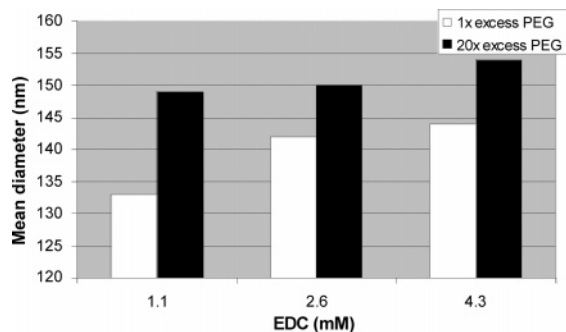
Table 1. Molecular Weights of Fmoc-PEG₅₀₀₀-NHS and Gal-PEG₅₀₀₀-NH₂ for Incremental Numbers of Ethylene Oxide Repeat Units, with Sodium Counterion for Comparison to Peaks of MALDI-TOF Spectra

<i>n</i>	predicted MW _{Fmoc-PEG-NH} + Na ⁺	observed MW _{Fmoc-PEG-NHS} + Na ⁺	predicted MW _{Gal-PEG-NH₂} + Na ⁺	observed MW _{Gal-PEG-NH₂} + Na ⁺
111	5318.1	5320.4	5251.3	5250.8
112	5362.0	5364.2	5296.3	5294.3
113	5406.1	5408.7	5340.3	5337.9
114	5450.1	5452.7	5384.3	5382.2
115	5494.1	5496.7	5428.4	5426.6
116	5538.1	5540.6	5472.4	5470.7
117	5582.2	5585.1	5516.4	5514.7
118	5626.2	5628.7	5560.4	5558.4
119	5670.2	5672.8	5604.5	5602.1
120	5714.2	5716.9	5648.5	5646.0
121	5758.3	5761.5	5692.5	5691.0
122	5802.3	5805.1	5736.5	5733.1

The primary population of peaks in Figure 2 is from $[M + Na]^+$, while the subpopulation comes from $[M + H]^+$. In addition to MALDI-TOF, the average molecular weight per galactose of the final product was determined to be about 5500 with the Amplex Red Galactose Assay Kit, as expected for nearly complete galactosylation of the PEG. Thus, the molecular weight determined from this technique compares well with the results of MALDI-TOF analysis.

PEGylated Nanoparticle Synthesis and Characterization. Most previous reports of PEGylating carboxy-polystyrene nanoparticles used 1 μ m beads or larger (17–20). These large particles are relatively insensitive to reaction conditions, and broadening of particle size distribution was not reported. Ploehn and Goodwin (21) PEGylated smaller carboxy-polystyrene beads (115 and 347 nm diameter), but no indication was given that polydispersity was monitored during that reaction. For the current purpose of determining physicochemical design parameters for next generation gene delivery vectors, polydispersity of the final PEGylated nanoparticles should be low, monomodal, and well-defined. We were interested in working with nanoparticles with hydrodynamic diameters in the range of about 45–150 nm. These relatively small polystyrene beads were found to be much more sensitive to reaction conditions than larger 200 nm beads, thus requiring careful study to identify reaction and purification conditions that resulted in pure nanoparticles with desired mean diameter, particle size distribution, and extent of surface PEGylation.

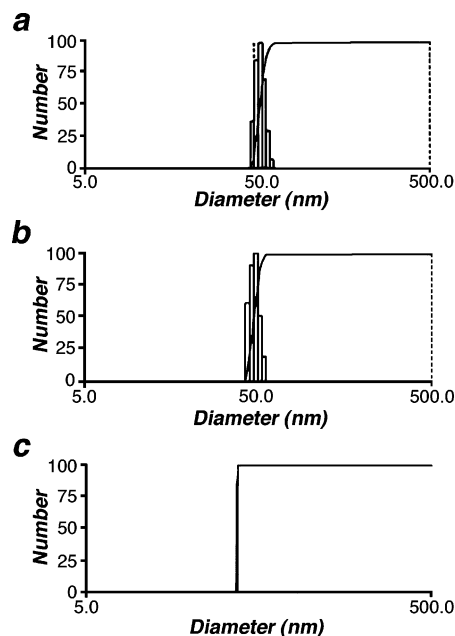
The extent of PEGylation, and hence the final nanoparticle hydrodynamic diameter, was controlled by varying the concentrations of PEG and EDC during nanoparticle synthesis, as shown by the results given in Figure 3. While varying the concentration of PEG in the reaction simply shifted the final mean particle size without affecting the distribution, EDC concentrations

**Figure 3.** Mean hydrodynamic diameters following PEGylation of 105 nm Fluospheres with different reagent concentrations.

above about 15 mM resulted in significant broadening of the particle size distribution.

By carefully controlling reaction conditions, nanoparticles could be synthesized with size distributions (Figure 4b) that closely match those of the cyclodextrin-based gene delivery particles (Figure 4a) they intend to mimic. PEGylated nanoparticles larger than 105 nm can be synthesized with very tight monodisperse distributions under appropriate reaction conditions (Figure 4c). The polydispersity of the 50 nm nanoparticles and polyplexes is about 0.06, while that of the 140 nm nanoparticles is about 0.005. Low polydispersities such as these allow the effect of nanoparticle size on biodistribution to be clearly determined.

TEM imaging of unmodified nanoparticles validated the particle sizes measured by photon correlation spectroscopy (PCS). Particle size of unmodified polystyrene nanoparticles was found to be in good agreement between TEM and PCS measurements. This was expected, given the spherical shape of the particles and hence the appropriateness of the Stokes–Einstein expression to relate the diffusion coefficient, which is measured by PCS, to the particle size. Further, PCS measurements of particle size were performed at various concentrations

**Figure 4.** Histograms of nanoparticle hydrodynamic diameter distributions, as measured by PCS in 150 mM NaCl, for (a) 50 nm PEGylated polyplexes, (b) 50 nm PEGylated nanoparticles, and (c) 140 nm PEGylated nanoparticles.

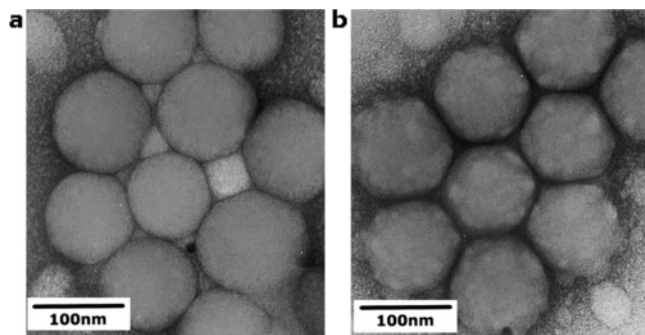


Figure 5. TEM images of (a) unmodified 105 nm Fluosphere nanoparticles and (b) PEGylated 105 nm polystyrene nanoparticles.

to ensure the accuracy of the reported result (22), and insignificant difference was found between these measurements.

As seen in the TEM images in Figure 5a, unmodified polystyrene Fluospheres adopt a close-packed arrangement with direct polystyrene-polystyrene contact between beads, while PEGylated nanoparticles (Figure 5b) are separated by darkly stained PEG coronas and avoid polystyrene-polystyrene contact. Because the nanoparticles must be dried for TEM analysis, the PEG layer is dehydrated and the diameter of PEGylated nanoparticles as determined by TEM is significantly smaller than their hydrodynamic diameter. Further evidence of consistent surface PEGylation was provided by our inability to separate PEGylated polystyrene nanoparticles into multiple populations by hydrophobic interaction chromatography, as described by Gbadamosi et al. (23). Moghimi demonstrated (24) that it is critical for the entire nanoparticle surface to be PEGylated to minimize nonspecific uptake of nanoparticles by the reticuloendothelial system. It is also important that the PEGylated nanospheres be well-shielded to avoid aggregation in serum. Additionally, the monodispersity of the 105 nm Fluospheres is evident from this image.

The stability of aqueous suspensions of 220 nm PEGylated polystyrene nanoparticles has been shown to increase dramatically for particles with hydrodynamic layer thicknesses of between 10 and 15 nm (25). The impact of PEGylated surfaces is even more critical in salt solution, where the Debye screening length will be much shorter than the hydrodynamic layer thickness. In 150 mM NaCl, for example, the Debye screening length is about 0.8 nm. As such, any charge-charge repulsion that originated from the particle surface in pure water will no longer be influential, and the PEG layer is entirely responsible for sterically shielding the particles. In the present work, 140 nm PEGylated nanoparticles were synthesized by grafting PEG onto 105 nm polystyrene nanoparticles, resulting in hydrodynamic layer thickness of slightly more than 15 nm. As such, this PEG corona is expected to provide near maximum protection against nanoparticle flocculation. Similarly, 50 nm PEGylated nanoparticles synthesized from 28 nm polystyrene have approximate hydrodynamic layer thicknesses of 11 nm. The decreased hydrodynamic thickness of PEG with the same molar mass on the smaller beads can be explained by the increased available angular segment volume with increased surface curvature (26). PEG₅₃₀₀ has a radius of gyration of 3.2 nm and an interfacial overlap concentration, $\sigma_{ol} = (\pi R_g^2)^{-1} = 0.031$ chains/nm² (27). The nanoparticles used in this study have a PEG surface density of about 0.14 chains/nm², that is much higher than σ_{ol} so it is expected that significant interactions are

Table 2. Fifty-Nanometer PEGylated Nanoparticles with Different Surface Densities of Galactose for Use in RCA120 Agglutination Assay

no. of beads per experiment	no. of galactose per bead	pmol galactose per cm ²	total no. of galactose per experiment	total no. of RCA ₁₂₀ binding sites per experiment
5.4×10^{12}	1142	81.3	6.2×10^{15}	9.5×10^{14}
5.4×10^{12}	556	39.6	3.0×10^{15}	9.5×10^{14}
5.4×10^{12}	357	25.4	1.9×10^{15}	9.5×10^{14}
5.4×10^{12}	183	13.0	9.9×10^{14}	9.5×10^{14}
5.4×10^{12}	0	0	0	9.5×10^{14}

occurring between polymer chains on the nanoparticle surface. This interaction manifests itself as a PEG layer that is considerably thicker than $2R_g$, the expected PEG thickness in the absence of polymer chain interaction.

Availability of Galactose for Receptor Binding.

As discussed earlier, galactose was used as a targeting ligand on some of the PEGylated nanoparticles. The surface density of galactose on the nanoparticles can be controlled by varying the ratio of Gal-PEG₅₀₀₀-NH₂ to MeO-PEG₅₀₀₀-NH₂ in the reaction. Further, the overall ratio of PEG-NH₂ to carboxylate groups enabled nanoparticles with different galactose moieties to be presented on the surface of nanoparticles through attachment via a 5000 Da PEG chain. To test whether the galactose moieties are accessible to bind large proteins, the particles were exposed to RCA₁₂₀. RCA₁₂₀ is a 120 000 Da lectin with two identical and independent galactose binding sites per molecule (28). Five 50 nm PEGylated nanoparticles were synthesized for this study with different surface densities of galactose, as shown in Table 2. When RCA₁₂₀ lectin is mixed with an appropriate number of galactosylated nanoparticles, agglutination is expected to occur. This effect is schematically illustrated in Figure 6, where lectins can be seen cross-linking galactosylated nanoparticles. This cross-linked network scatters light, and progress of agglutination can be monitored by measuring absorbance at 560 nm. Agglutination should be rapidly reversible by the addition of free galactose.

By fixing the numbers of lectin molecules and nanoparticles in all experiments, the effect of galactose surface density on agglutination can be seen (Figure 7). Turbidity, expressed as absorbance at 560 nm, is found to increase more quickly and to a greater extent for nanoparticles with a higher surface density of galactose than for comparable nanoparticles with lower surface densities of galactose. For nanoparticles with less than about 13 pmol galactose/cm², there are comparable numbers of galactose binding sites available on the RCA₁₂₀ lectin and galactose available on the surface of nanoparticles, and no agglutination is observed. While this result may indicate that all galactose molecules are not accessible to binding, the general availability of nanoparticle-bound galactose for protein binding is confirmed for the higher values.

As compared to the rapid network disruption associated with galactose addition to the agglutinated solution (Figure 7), addition of an equal volume and concentration of glucose does not disrupt the cross-linked network (Figure 8). The only effect caused by addition of 100 μ L of a glucose solution to the cuvette is related to dilution and is identical to the effect of adding 100 μ L of water. It is thus confirmed that agglutination is due to interaction between nanoparticle-bound galactose and RCA₁₂₀ lectin molecules.

Description of Nanoparticles for Uptake Studies.

It has thus far been demonstrated that nanoparticles can

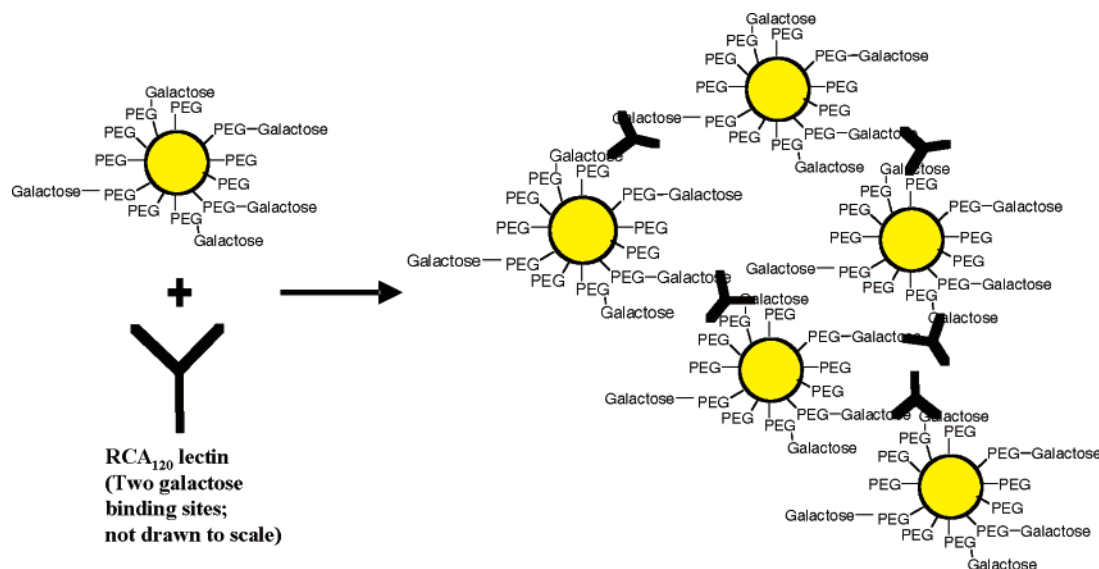


Figure 6. Schematic illustration of nanoparticle agglutination as a result of RCA₁₂₀ lectin binding galactosylated nanoparticles.

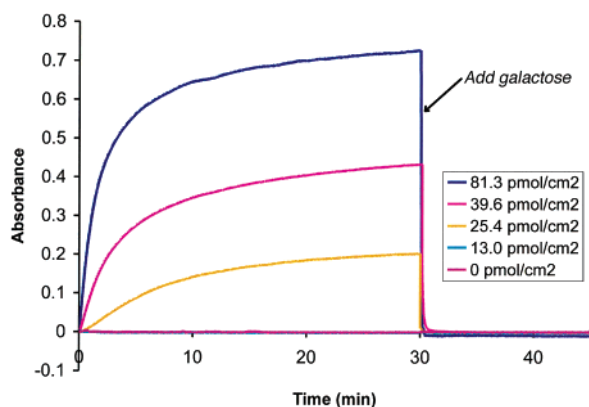


Figure 7. Turbidity increase due to agglutination of galactosylated 50 nm nanoparticles with RCA₁₂₀ lectin. Galactose (100 μ L of 140 mM solution) in PBS is added at 30 min.

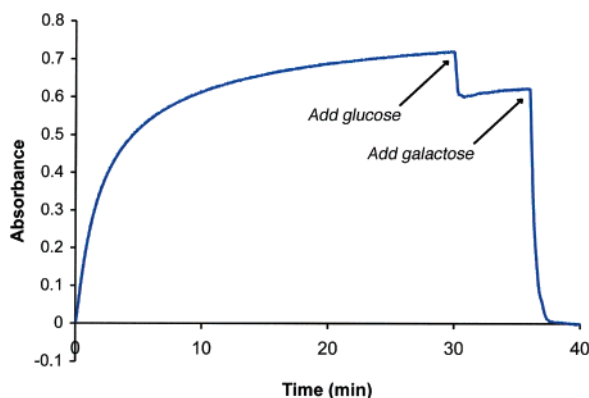


Figure 8. Turbidity increase of 50 nm nanoparticle with 81.3 pmol/cm² surface galactose density due to agglutination with RCA₁₂₀ lectin. Glucose (100 μ L of 140 mM solution) in PBS is added at 30 min, and then 100 μ L of 140 mM galactose in PBS is added at 35 min.

be synthesized with a wide range of physicochemical properties. However, a select few must be chosen for in vitro and in vivo uptake experiments. Four nanoparticles were selected for this role, and their properties are detailed in Table 3.

Nanoparticles with mean diameters of 50 and 140 nm were selected for use because (1) cyclodextrin-based gene delivery particles can be conveniently synthesized in the

Table 3. Summary of Physicochemical Properties of the Four Nanoparticles To Be Used in Uptake Experiments

bead name	mean diameter (nm)	ζ -potential (mV)	galactose surface density (pmol/cm ²)
Gal-50	51.5	-2.7 ± 1.8	25.4
MeO-50	53.5	-2.7 ± 2.8	0
Gal-140	138.1	-2.6 ± 2.1	30.6
MeO-140	138.7	-3.2 ± 2.3	0

range of about 45 nm to about 150 nm, so the nanoparticles selected for use in the present study approximate the bounds of that range, (2) access to hepatocytes through the hepatic sinusoidal wall requires passage through endothelial-cell pores that are estimated at 150–200 nm (29), and (3) 50 nm is below the 70 nm cutoff that has been proposed for neutral liposome uptake via ASGPr (30). The effect of galactose presentation on the surface of the nanoparticles were investigated for 50 and 140 nm nanoparticles with galactose surface densities of 25–30 pmol/cm². Galactosylated 50 and 140 nm nanoparticles are referred to as Gal-50 and Gal-140. The equivalent nontargeted nanoparticles have methoxy terminated PEG chains and are referred to as MeO-50 and MeO-140.

All nanoparticles in Table 3 have slightly anionic surface potentials (at the plane of hydrodynamic shear) to minimize nonspecific uptake. Cationic particles are internalized nonspecifically through proteoglycan receptors and may stick to anionic cell surface membranes, while highly anionic polystyrene nanoparticles have increased nonspecific uptake by scavenger receptors following complement activation (31, 32). Unmodified, carboxylated, polystyrene beads (as-received starting material) have ζ -potentials of approximately -45 mV. The PEGylated nanoparticles have mean ζ -potentials of about -3 mV. These surfaces are nearly neutral due to the combined effect of carboxylate group conversion to amides on the nanoparticle surfaces and PEG shielding of the surface charge.

Serum Aggregation of PEGylated Nanoparticles.

To investigate the effect of particle size on specific uptake phenomena, the nanoparticles must remain dispersed in the presence of serum. They also must not bind serum opsonins with great affinity, as such binding has been shown to increase the hepatic uptake of 50 and 500 nm polystyrene nanoparticles (33).

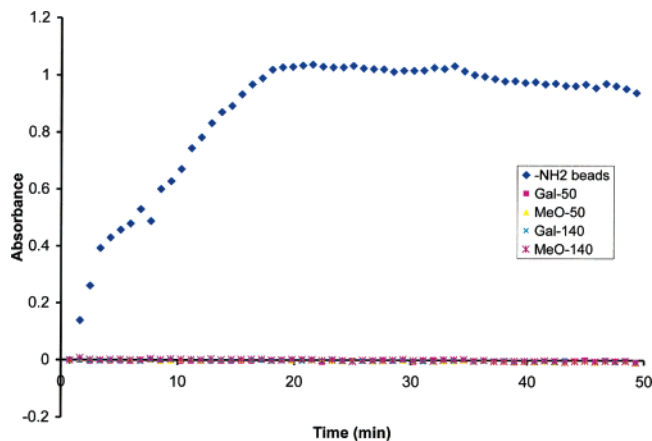


Figure 9. Nanoparticle aggregation in the presence of active mouse serum.

If serum proteins bind the surface of nanoparticles, cross-linking between nanoparticles would be expected to occur. Since many serum proteins are anionic, cross-linking should be more significant for cationic nanoparticles. For this reason, amino-modified polystyrene nanoparticles were used as a positive control in serum stability studies. As shown by the data in Figure 9, amine-functionalized nanoparticles cross-linked quickly and extensively in active mouse serum, while the PEGylated nanoparticles did not. The role of serum proteins in inducing aggregation of the amine-functionalized nanoparticles is supported by the lack of aggregation of any of the nanoparticles in PBS. Despite considerable effort, aggregation of the PEGylated nanoparticles could not be induced under any conditions.

CONCLUSIONS

Here, we report the synthesis and characterization of PEGylated polystyrene nanoparticles. These nanoparticles have slightly anionic surface potentials to minimize nonspecific interactions with cells and tissues in vivo. The synthetic scheme allows for the variation of mean particle size and particle size distribution through changes in reaction conditions. The nanoparticle synthesis is also amenable to incorporation of various ligand types with variable surface densities. The synthesized nanoparticles are shown to have PEGylated surfaces that resist aggregation in serum. Finally, the availability of galactose to receptor binding is demonstrated by agglutination with RCA₁₂₀.

Nanoparticles were synthesized here specifically for the purpose of identifying design constraints to guide next generation gene delivery to the liver. In preparation for in vitro and in vivo uptake experiments, four nanoparticles were prepared: Gal-50 and Gal-140 that are galactosylated 50 and 140 nm nanoparticles, and MeO-50 and MeO-140 that are methoxy-terminated 50 and 140 nm nanoparticles. Through the use of these nanoparticles, the effects of nanoparticle size and presence of galactose on the nanoparticle surface on the biodistribution in liver are explored in Part 2 of this work (16).

LITERATURE CITED

- (1) Verma, I. M., and Somia, N. (1997) Gene therapy – promises, problems and prospects. *Nature* 389, 239–242.
- (2) Prieto, J., Qian, C., Hernandez-Alcoceba, R., Gonzalez-Asequinolaza, G., Mazzolini, G., Sangro, B., and Kramer, M. G. (2004) Gene therapy of liver diseases. *Expert Opin. Biol. Ther.* 4, 1073–1091.
- (3) Kren, B. T., Chowdhury, N. R., Chowdhury, J. R., and Steer, C. J. (2002) Gene therapy as an alternative to liver transplantation. *Liver Transplant.* 8, 1089–1108.
- (4) Walsh, C. E. (2003) Gene therapy Progress and Prospects: Gene therapy for the hemophilias. *Gene Ther.* 10, 999–1003.
- (5) Shlomai, A., and Shaul, Y. (2004) RNA interference – small RNAs effectively fight viral hepatitis. *Liver Int.* 24, 526–531.
- (6) Germain, D. P. (2004) Gaucher's disease: a paradigm for interventional genetics. *Clin. Genet.* 65, 77–86.
- (7) Mishra, S., Webster, P., and Davis, M. E. (2004) PEGylation significantly affects cellular uptake and intracellular trafficking of nonviral gene delivery particles. *Eur. J. Cell Biol.* 83, 97–111.
- (8) Moghimi, S. M., and Patel, H. M. (1998) Serum-mediated recognition of liposomes by phagocytic cells of the reticuloendothelial system – The concept of tissue specificity. *Adv. Drug Delivery Rev.* 32, 45–60.
- (9) Dan, C., and Wake, K. (1985) Modes Of Endocytosis Of Latex-Particles In Sinusoidal Endothelial And Kupffer Cells Of Normal And Perfused Rat-Liver. *Exp. Cell Res.* 158, 75–85.
- (10) Dunn, S. E., Brindley, A., Davis, S. S., Davies, M. C., and Illum, L. (1994) Polystyrene-Poly(Ethylene Glycol) (Ps-Peg2000) Particles As Model Systems For Site-Specific Drug-Delivery. 2. The Effect Of Peg Surface-Density On The In-Vitro Cell-Interaction And In-Vivo Biodistribution. *Pharm. Res.* 11, 1016–1022.
- (11) Davis, M. E., Pun, S. H., Bellocq, N. C., Reineke, T. M., Popielarski, S. R., Mishra, S., and Heidel, J. D. (2004) Self-assembling nucleic acid delivery vehicles via linear, water-soluble, cyclodextrin-containing polymers. *Curr. Med. Chem.* 11, 179–197.
- (12) Pun, S. H., and Davis, M. E. (2002) Development of a nonviral gene delivery vehicle for systemic application. *Bioconjugate Chem.* 13, 630–639.
- (13) Reineke, T. M., and Davis, M. E. (2003) Structural effects of carbohydrate-containing polycations on gene delivery. 1. Carbohydrate size and its distance from charge centers. *Bioconjugate Chem.* 14, 247–254.
- (14) Reineke, T. M., and Davis, M. E. (2003) Structural effects of carbohydrate-containing polycations on gene delivery. 2. Charge center type. *Bioconjugate Chem.* 14, 255–261.
- (15) Popielarski, S. R., Mishra, S., and Davis, M. E. (2003) Structural effects of carbohydrate-containing polycations on gene delivery. 3. Cyclodextrin type and functionalization. *Bioconjugate Chem.* 14, 672–678.
- (16) Popielarski, S. R., Hu-Lieskovan, S., French, S. W., Triche, T. J., and Davis, M. E. (2005) A Nanoparticle-Based Model Delivery system to Guide the Rational Design of Gene Delivery to the Liver. 2. In Vitro and In Vivo Uptake Results. *Bioconjugate Chem.* 16, 1071–1080.
- (17) VanDelden, C. J., Bezemer, J. M., Engbers, G. H. M., and Feijen, J. (1996) Poly(ethylene oxide)-modified carboxylated polystyrene latices – Immobilization chemistry and protein adsorption. *J. Biomat. Sci.-Polym. E.* 8, 251–268.
- (18) Meng, F. H., Engbers, G. H. M., and Feijen, J. (2004) Polyethylene glycol-grafted polystyrene particles. *J. Biomed. Mater. Res.-A* 70A, 49–58.
- (19) Meng, F. H., Engbers, G. H. M., Gessner, A., Muller, R. H., and Feijen, J. (2004) Pegylated polystyrene particles as a model system for artificial cells. *J. Biomed. Mater. Res.-A* 70A, 97–106.
- (20) Valentine, M. T., Perlman, Z. E., Gardel, M. L., Shin, J. H., Matsudaira, P., Mitchison, T. J., and Weitz, D. A. (2004) Colloid surface chemistry critically affects multiple particle tracking measurements of biomaterials. *Biophys. J.* 86, 4004–4014.
- (21) Ploehn, H. J., and Goodwin, J. W. (1990) Rheology Of Aqueous Suspensions Of Polystyrene Latex Stabilized By Grafted Poly(Ethylene Oxide). *Faraday Discuss.* 90, 77–90.
- (22) Dejaeger, N., Demeyere, H., Finsy, R., Sneyers, R., Vanderdeelen, J., Vandermeeren, P., and Vanlaethem, M. (1991) Particle Sizing By Photon-Correlation Spectroscopy. 1. Monodisperse Lattices – Influence Of Scattering Angle And Concentration Of Dispersed Material. *Part. Part. Syst. Character.* 8, 179–186.

- (23) Gbadamosi, J. K., Hunter, A. C., and Moghimi, S. M. (2002) PEGylation of microspheres generates a heterogeneous population of particles with differential surface characteristics and biological performance. *FEBS Lett.* 532, 338–344.
- (24) Moghimi, S. M. (2002) Chemical camouflage of nanospheres with a poorly reactive surface: towards development of stealth and target-specific nanocarriers. *Biochim. Biophys. Acta (Mol. Cell Res.)* 1590, 131–139.
- (25) Wind, B., and Killmann, E. (1998) Adsorption of poly(ethylene oxide) on surface modified silica stability of bare and covered particles in suspension. *Colloid Polym. Sci.* 276, 903–912.
- (26) Killmann, E., and Sapuntzjis, P. (1994) Dynamic Light-Scattering Of Polystyrene Latex And Silica With Adsorbed Poly(Ethylene Oxide) Layers – Influence Of Ionic-Strength And Coverage. *Colloids Surface. A* 86, 229–238.
- (27) Devanand, K., and Selser, J. C. (1991) Asymptotic-Behavior And Long-Range Interactions In Aqueous-Solutions Of Poly(Ethylene Oxide). *Macromolecules* 24, 5943–5947.
- (28) Van Wauwe, J. P., Loontjens, F. G., and Debruyne, C. K. (1973) Interaction Of Ricinus-Communis Hemagglutinin With Polysaccharides And Low-Molecular Weight Carbohydrates. *Biochim. Biophys. Acta* 313, 99–105.
- (29) Wisse, E., Dezanger, R. B., Charels, K., Vandersmissen, P., and McCuskey, R. S. (1985) The Liver Sieve – Considerations Concerning The Structure And Function Of Endothelial Fenestrae, The Sinusoidal Wall And The Space Of Disse. *Hepatology* 5, 683–692.
- (30) Rensen, P. C. N., Sliedregt, L., Ferns, A., Kieviet, E., van Rossenberg, S. M. W., van Leeuwen, S. H., van Berkel, T. J. C., and Biessen, E. A. L. (2001) Determination of the upper size limit for uptake and processing of ligands by the asialoglycoprotein receptor on hepatocytes in vitro and in vivo. *J. Biol. Chem.* 276, 37577–37584.
- (31) Gref, R., Miralles, G., and Dellacherie, E. (1999) Polyoxyethylene-coated nanospheres: effect of coating on zeta potential and phagocytosis. *Polym. Int.* 48, 251–256.
- (32) Ogawara, K., Yoshida, M., Higaki, K., Kimura, T., Shiraishi, K., Nishikawa, M., Takakura, Y., and Hashida, M. (1999) Hepatic uptake of polystyrene microspheres in rats: Effect of particle size on intrahepatic distribution. *J. Controlled Release* 59, 15–22.
- (33) Ogawara, K., Yoshida, M., Takakura, Y., Hashida, M., Higaki, K., and Kimura, T. (1999) Interaction of polystyrene microspheres with liver cells: roles of membrane receptors and serum proteins. *Biochim. Biophys. Acta (Gen. Subjects)* 1472, 165–172.

BC050113D